





Tilted Dirac cones and asymmetric conical diffraction in photonic Lieb-kagome latticesJean-Philippe Lang ^{*}, Haissam Hanafi ^{*,†}, Jörg Imbrock , and Cornelia Denz
Institute of Applied Physics, University of Münster, 48149 Münster, Germany (Received 8 November 2022; accepted 30 January 2023; published 9 February 2023; corrected 20 March 2023)

The Lieb lattice and the kagome lattice, which are both well known for their Dirac cones and flat bands, can be continuously converted into each other by a shearing transformation. During this transformation, the flat band is destroyed, but the Dirac cones remain and become tilted, with types I, II, and III occurring for different parameters. In this work, we first study these tilted Dirac cones using a tight-binding model, revealing how they can be engineered into the different types. We then demonstrate conical diffraction in a photonic lattice realization of the Lieb-kagome lattice using split-step beam propagation simulations, obtaining evidence of the presence of Dirac cones tilted in different directions. Finally, we performed experiments with photonic lattices laser written in fused silica (SiO_2) to validate the results of the simulations. These studies advance the understanding of the Lieb-kagome lattice and tilted Dirac cones in general and provide a basis for further research into this interesting tunable lattice system.

DOI: [10.1103/PhysRevA.107.023509](https://doi.org/10.1103/PhysRevA.107.023509)**I. INTRODUCTION**

A Dirac cone is an intersection of (energy) bands in a single point, the Dirac point, surrounded by linear dispersion, thus forming cones in the band structure. In particular, since the discovery of graphene [1], in which Dirac cones exist, they have been the focus of both theoretical and experimental research interest [2–5]. Aside from the regular Dirac cones found, among others, in graphene, there exist also more exotic Dirac cones, such as higher order conical intersections [6–8] and tilted Dirac cones [9–11]. Tilted Dirac cones can be classified according to their degree of tilting into weakly tilted (type I), strongly tilted (type II), and critically tilted (type III) cones [9]. Type III cones in particular remain challenging to observe in solid-state physics, although some candidates for a realization have recently been suggested [12,13]. Since the origin of Dirac cones lies in lattice symmetries, however, they are fundamental phenomena, which can occur in any periodic system. One such system that is of particular interest due to its versatility is a photonic lattice, which consists of a periodic arrangement of weakly coupled single-mode waveguides [14]. Using fabrication techniques such as direct laser writing, arbitrary lattice geometries in different host materials can be realized [15–17]. By varying the shape of the constituting waveguides in a photonic lattice, one can simulate the influence of electrical fields, realizing phenomena such as Floquet topological insulators [18], Bloch-Zener oscillations [19], and dynamic localization [20]. Recently, even experimental evidence of type III Dirac cones has been found in a photonic lattice system [9].

Spatial light evolution in a photonic lattice is described by the paraxial wave equation, which is mathematically equivalent to a time-dependent Schrödinger equation. Therefore, photonic lattices can be used as model systems for the time

evolution of the electron-wave function in two-dimensional (2D) materials. In photonic lattices, the presence of Dirac cones leads to a phenomenon known as conical diffraction, in which a ring of light with constant thickness and linearly growing diameter is observed. Such conical diffraction has been shown in experiments for regular Dirac cones [21,22]. Conical diffraction from tilted Dirac cones was recently demonstrated in simulations [23].

The Lieb lattice and the kagome lattice are two types of artificial lattices, which have long been studied theoretically, because they feature both Dirac cones and completely dispersionless flat bands. They can be easily realized as photonic lattices, and as such have been studied in the context of localized (flat band) states [24–26], conical diffraction [22,27,28], and topological insulators [29]. The Lieb and the kagome lattices are related by a shearing transformation and can be continuously transformed into each other. Such a Lieb-kagome model was, to our knowledge, first proposed in 2011 [30], and recently Jiang *et al.* [31] published a study on this lattice system focusing on the topological effects caused by breaking the time-reversal symmetry. Soon after, Lim *et al.* [32] released a detailed theoretical study on the splitting of Dirac cones during the transition from Lieb to the kagome lattice. So far none of the works on the Lieb-kagome lattice contain simulations or experiments that could verify the numerical results. Furthermore, the variable tilting of the Dirac cones of this lattice system has not yet been studied systematically. Doing so would reveal ways to engineer not only the rather common tilted type I Dirac cones, but also the more rare type II and III cones. Type II Dirac cones can be used in photonic lattices to study several interesting phenomena, such as Klein tunneling [33], topological valley Hall states [34], and more. Type III cones are of interest as a model system for a black hole event horizon [12,35]. To fill these gaps, in this work, we first study the Lieb-kagome lattice with tight-binding calculations, focusing on the variable tilting of its Dirac cones, showing how it can be tailored to realize

^{*}J.-P.L. and H.H. contributed equally to this work.[†]haissam.hanafi@uni-muenster.de

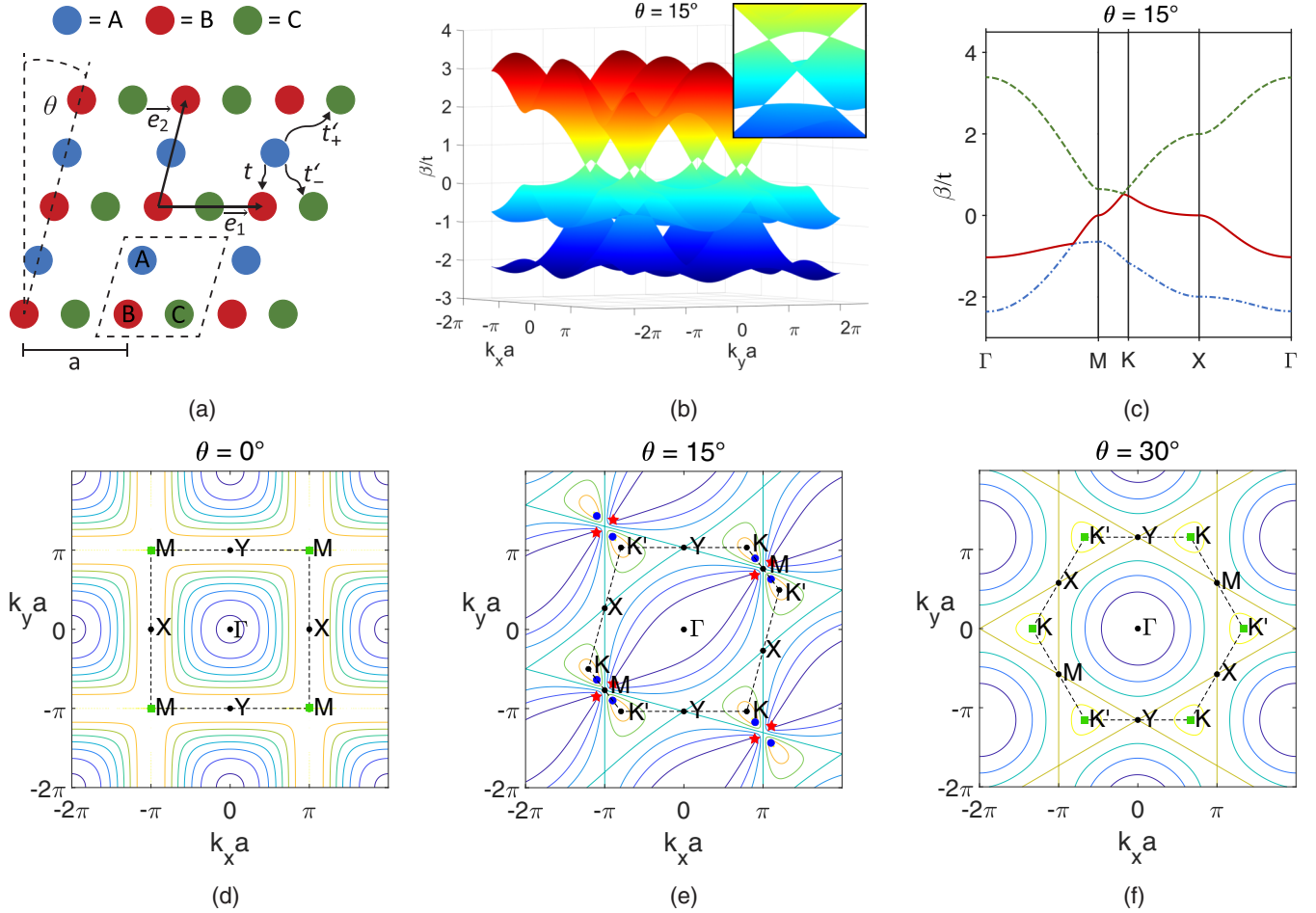


FIG. 1. The Lieb-kagome lattice: (a) Sketch of the Lattice geometry. (b) Tight-binding band structure of a Lieb-kagome lattice with $\theta = 15^\circ$. The inset shows a close-up of four pairs of Dirac cones from different angles. (c) Projection of the band structure from panel (b) on lines between high-symmetry points. [(d)–(f)] Contour plots of the middle bands of Lieb-kagome lattices with different shearing angles θ . The first Brillouin zones are indicated as dashed black lines along with some high-symmetry points. Dirac points are indicated in green squares for regular Dirac cones, blue filled circles for the upper tilted Dirac cones, and red stars for the lower tilted Dirac cones.

type I, II, and III Dirac cones. After that, we demonstrate asymmetric conical diffraction in photonic Lieb-kagome lattices, resulting from differently tilted Dirac cones, by performing simulations based on the split-step algorithm [36]. Lastly, we perform experiments in laser-written photonic lattices, testing the results of the previous simulations.

II. THE LIEB-KAGOME LATTICE

A. Tight-binding model

Although the Lieb and the kagome lattice belong to different symmetry groups, they share the structure of their unit cells, which consist of one corner site and two edge-centered sites [31], making them interconvertible through a shearing transformation. Therefore, both lattices can be combined into a single unified model, which is sketched in Fig. 1(a). In this Lieb-kagome model, we label the edge-center sites as A and C and the corner sites as B. The lattice constant a is the distance between unit cells, making the nearest neighbor distance $a/2$. The parameter that describes the transition between the Lieb and kagome lattice is the shearing angle labeled θ . This angle can be varied between 0° , at which

point the model is equivalent to the Lieb lattice, and 30° , where the model represents the kagome lattice. In our calculations, we consider nearest neighbor interaction, which occurs between lattice sites labeled A and B and between B and C, and next-nearest neighbor interaction between A and C sites. At $\theta = 0^\circ$ (Lieb lattice), every lattice site A has four C sites as next-nearest neighbors, all with the same distance. When θ increases, the distance to two of those C sites increases, while the distance to the other two decreases. At $\theta = 30^\circ$ (kagome lattice), an A lattice site has two C sites as nearest neighbors and two as next-nearest neighbors. To describe the Lieb-kagome lattice, we therefore need three coupling constants: The nearest neighbor coupling constant t and the next-nearest neighbor coupling constants t'_\pm for the case of increasing (t'_+) or decreasing (t'_-) distances when θ is increased, as indicated in Fig. 1(a). To describe the distance dependence of the coupling constants, we adopt a model from Ref. [31] to describe the relative coupling strength γ :

$$\frac{t'}{t} \equiv \gamma = \left[\exp\left(\frac{d_{\text{NN}} - d_{\text{NNN}}}{d_{\text{NN}}}\right) \right]^{n_{\text{exp}}}. \quad (1)$$

Here, d_{NN} and d_{NNN} are the distances of nearest neighbor and next-nearest neighbor, respectively, while the exponent n_{exp} is a free parameter that determines how quickly the coupling decreases with distance. In our later performed simulations of conical diffraction, we found $n_{\text{exp}} = 4$ to best describe our realistic photonic lattice system, as at that value clear ring patterns could be observed for all θ between 0° and 30° . Therefore, we used that value for all subsequent calculations, with the exception of the contour plots presented here, where we used $n_{\text{exp}} = 8$, because that value allows the movement of the Dirac cones to be seen more clearly. However, this value for n_{exp} is still realistic for photonic lattices, particularly if the excitation uses a larger wavelength than we used in our simulations. Furthermore, the directions of movement of the Dirac cones and the conclusions drawn from it remain the same regardless of the specific value.

For the Lieb-kagome model shown in Fig. 1(a), some simple geometric considerations lead to

$$\frac{t'_\pm}{t} \equiv \gamma_\pm = [\exp(1 - \sqrt{2 \pm 2 \sin \theta})]^{n_{\text{exp}}}. \quad (2)$$

After those deliberations, we can now calculate a momentum-space tight-binding Hamiltonian for the Lieb-kagome lattice:

$$H(\mathbf{k}) = 2t \begin{pmatrix} 0 & AB & AC \\ AB & 0 & BC \\ AC & BC & 0 \end{pmatrix}, \quad (3)$$

with the matrix elements

$$AB = \cos\left(\frac{ak_x \sin \theta + ak_y \cos \theta}{2}\right), \quad (4a)$$

$$AC = \gamma_- \cos\left(\frac{ak_x(1 - \sin \theta) - ak_y \cos \theta}{2}\right) + \gamma_+ \cos\left(\frac{ak_x(1 + \sin \theta) + ak_y \cos \theta}{2}\right), \quad (4b)$$

$$BC = \cos\left(\frac{ak_x}{2}\right), \quad (4c)$$

corresponding to the interaction between the respective lattice sites. Diagonalizing this Hamiltonian yields three eigenvalues $\beta(k_x, k_y)$. In a solid-state system, such eigenvalues represent the energy bands that describe the electron dynamics of the lattice. In a model system such as a photonic lattice, which we will consider later, they give us the diffraction relation $k_z(k_x, k_y)$.

B. Band evolution

Figures 1(b) and 1(c) show the band structure and projection of it on lines between high-symmetry points of a Lieb-kagome lattice with $\theta = 15^\circ$, respectively. It can be seen that in transition states between Lieb and kagome lattices there is no longer a flat band, but there are several Dirac cones, which are clearly tilted. The Dirac points in transition states can be distinguished into those situated at positive β and those at negative β , which we will call in the following upper and lower Dirac points and /cones, respectively.

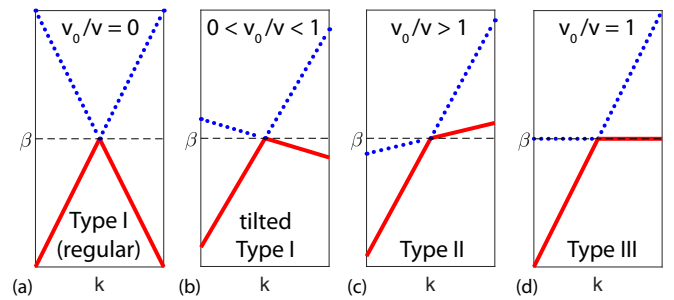


FIG. 2. Classification of tilted Dirac cones in 1D by projecting them onto their tilt direction, which results in two intersecting lines (blue dashed and red). From the slopes of the lines, an effective tilt parameter v_0/v can be calculated and used to classify Dirac cones into types I, II, and III. Based on Ref. [9].

The movement of Dirac points in dependence on θ can be seen in Figs. 1(d)–1(f). Starting from the Lieb lattice ($\theta = 0^\circ$), there are Dirac points belonging to untilted Dirac cones at the four corners of the first Brillouin zone, the M points. When θ is increased, each of those Dirac points splits into four, two upper Dirac points which move along the M-K/K' direction and two lower Dirac points moving along the M- Γ direction. This movement of Dirac points along high-symmetry directions away from the high-symmetry points is known to cause the Dirac cones to tilt in the respective direction of movement [4,37]. When θ reaches 30° (kagome lattice), the lower Dirac points merge into a parabolic band touching, and the remaining six Dirac cones at the corners K/K' of the first Brillouin zone are again untilted.

III. TILTED DIRAC CONES

A. Classification of tilted Dirac cones

To classify the Dirac cones of the Lieb-kagome lattice by their tilting, we adapt a model from Ref. [9] to one dimension, considering a cut through a Dirac cone along its tilt direction. In our model, a Dirac cone is described by two intersecting lines with slopes of $s_1 = v_0 + v$ and $s_2 = v_0 - v$, respectively. Here the parameter v describes the cones' opening angle (being wider for smaller v), while a nonzero v_0 introduces a tilt to the cones. Dirac cones can be classified by their tilt into four types (see Fig. 2): Regular (untilted) type I cones, weakly tilted type I cones, strongly tilted type II cones, and critically tilted type III cones, which form the threshold between types I and II. In our model, this classification can be performed using an effective tilt parameter v_0/v as shown in Fig. 2.

Parameters v and v_0 can be calculated from a 1D band structure such as Fig. 1(c) by fitting its data with two lines in the vicinity of the Dirac point. With this the degree of tilting and classification of Dirac cones can be tracked while varying different parameters in the band structure calculations.

B. Evolution of tilted Dirac cones in the Lieb-kagome lattice

Figure 3(a) shows v_0 , corresponding to the degree of tilting, and v_0/v , the parameter used for classification, over the shearing angle θ for the upper and lower Dirac cones of the Lieb-kagome lattice. The edge cases of $\theta = 0^\circ$ and $\theta = 30^\circ$,

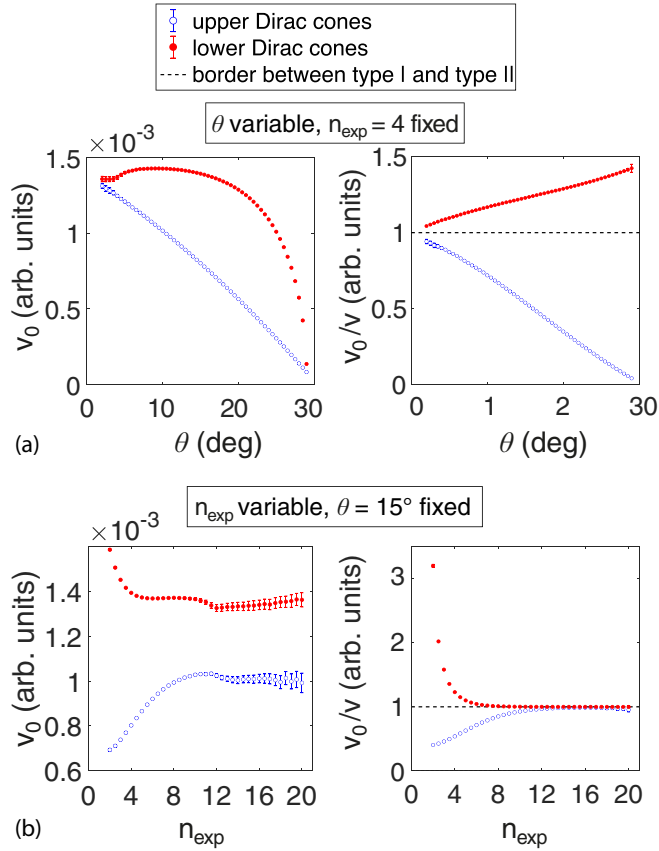


FIG. 3. Degree of tilting v_0 and effective tilt parameter v_0/v of the upper (blue empty circles) and lower Dirac (red filled circles) cones of the Lieb-kagome lattice: (a) as a function of θ and (b) as a function of n_{exp} . Error bars were calculated from the uncertainty of the fits performed to calculate these values.

as well as values of θ very close to them, were excluded. For both edge cases, there is only one type of Dirac cone with $v_0 = v_0/v = 0$ (i.e., no tilt), and for θ very close to those limits, there are not enough data points to perform reliable fits because the Dirac points are too close together.

The degree of tilting (v_0) of both types of Dirac cones is the highest and almost identical, for small θ . When θ increases, the tilt of the upper Dirac cones decreases almost linearly, while that of the lower Dirac cones resembles a curve of the form $y(x) = a - b \exp(cx)$, staying almost constant for low θ and rapidly decreasing for high θ , until the tilt of both types of Dirac cones vanishes as θ approaches 30° . For θ , aside from the edge cases, the lower Dirac cones are therefore always tilted more strongly than the upper cones.

The effective tilt parameter v_0/v approaches 1 for both upper and lower Dirac cones for low θ , meaning that they both approach the border case of critically tilted (type III) Dirac cones. For the upper Dirac cones, v_0/v decreases with rising θ , making them weakly tilted (type I) cones, while it increases for the lower Dirac cones, meaning they become strongly tilted (type II) cones.

Another parameter that can be used to influence the Dirac cones' tilt is n_{exp} , the parameter describing how quickly next-nearest neighbor coupling decays with the distance between lattice sites (a higher n_{exp} means that coupling decreases more

quickly). This could be influenced in experiments by tailoring the coupling between lattice elements, for example, in photonic lattices through the choice of parameters for writing waveguides or the excitation wavelength [38]. We therefore also calculated v_0 and v_0/v in dependence on n_{exp} with a fixed θ of 15° , the results of which are shown in Fig. 3(b).

Starting again with the degree of tilting, the lower Dirac cones show a stronger tilt for all values of n_{exp} . The difference between the two types of cone is the largest for small n_{exp} . With rising n_{exp} , v_0 initially increases for the upper Dirac cones and decreases for the lower Dirac cones, until both reach mostly constant values, which happens at a lower value of n_{exp} for the lower cones.

The difference in the effective tilt parameter of the upper and lower Dirac cones is also most pronounced for low n_{exp} , where again the upper Dirac cones are type I and the lower Dirac cones are type II. When n_{exp} increases, both the upper and lower Dirac cones approach type III cones, which again happens at a lower n_{exp} for the lower Dirac cones.

C. Discussion

We have shown how the shearing angle θ and the parameter n_{exp} can be used to influence the tilt of Dirac cones in the Lieb-kagome lattice, making it possible to tailor them to type I, II, or III Dirac cones. For most parameters, the upper Dirac cones are type I, the lower Dirac cones are type II cones, but both approach critically tilted type III cones for low θ or high n_{exp} . In both cases, however, the Dirac cones are very close together in \mathbf{k} space, making it difficult to excite and study them individually. Based on our studies, the best way to realize type III Dirac cones in the Lieb-kagome lattice is to increase n_{exp} , e.g., by decreasing the refractive index increment of the waveguides or increasing the excitation wavelength, until the lower Dirac cones approach type III, which happens at a lower n_{exp} than for the upper Dirac cones, so the Dirac cones are still well separated.

IV. ASYMMETRIC CONICAL DIFFRACTION

A. Photonic lattices and conical diffraction

Recently, both the Lieb and the kagome lattice have been realized as superlattices in electronic systems [39,40], but for a general freely tunable Lieb-kagome lattice such an approach would be unsuitable. A common way to study lattices with unconventional geometry is to use model systems. In particular, photonic lattices, which are periodic arrangements of weakly coupled waveguides, have been used to demonstrate a variety of phenomena known from solid-state physics. The evolution of light in such a photonic lattice can be described by the paraxial wave equation

$$\tilde{\lambda} \frac{\partial}{\partial z} \psi(x, y, z) - \left(\frac{\tilde{\lambda}^2}{2n_0} \nabla_{\perp}^2 + \Delta n(x, y, z) \right) \psi(x, y, z) = 0, \quad (5)$$

where $\psi(x, y, z)$ is the wave function, $\tilde{\lambda} = \lambda/2\pi$ is the reduced wavelength of light in the medium, n_0 is the refractive index of the medium, and $\Delta n(x, y, z) = n(x, y, z) - n_0$ is the refractive index increment between the waveguides and the

TABLE I. Summary of the parameters of the beam propagation simulations.

Waveguide diameter (FWHM)	3 μm
Maximal refractive index increment of waveguides	1.3×10^{-3}
Waveguide distance	20 μm
Excitation wavelength	700 nm
Diameter of excitation beam (FWHM)	100 μm
Propagation distance	60 mm

medium. This equation is mathematically equivalent to a time-dependent two-dimensional Schrödinger equation, with the most striking difference being that time is replaced by the propagation distance z . This means that spatial light evolution in a photonic lattice is equivalent to time evolution of the electron-wave function in a crystal lattice. In consequence, the dispersion relation $\beta(k_x, k_y)$ of a photonic Lieb-kagome lattice can be described by the same tight-binding model we introduced in Sec. II, which was originally developed for the Schrödinger equation. This justifies the usage of photonic lattices as a model system in experiments and simulations.

The presence of Dirac cones leads to a phenomenon called conical diffraction, where the lattice diffracts light into a ring with constant thickness and a radius which increases linearly with propagation distance. This was first demonstrated in simulations and experiments in 2007 by Peleg *et al.* [21] using a honeycomb lattice. Asymmetric conical diffraction arising from tilted Dirac cones was demonstrated in simulations by Zhong *et al.* in 2019 [23], who observed rings moving transversally in the tilt direction of the cones during propagation.

B. Beam propagation simulations of conical diffraction in the Lieb-kagome lattice

In order to verify the existence of tilted Dirac cones in the Lieb-kagome lattice, we studied conical diffraction in photonic lattices using a split-step beam propagation simulation. We chose the parameters of the simulation to be typical for photonic lattices produced by direct laser writing in fused silica. A summary of the most important parameters is provided in Table I.

In order to excite the Dirac cones of the lattice, the positions of the Dirac points in \mathbf{k} space were calculated and they were targeted with a superposition of plane waves with the corresponding phases. The resulting light field was then superimposed with a Gaussian beam in order to excite a finite region in \mathbf{k} space around the Dirac points and furthermore to leave enough space for the light to spread into the characteristic ring pattern. To observe full, unbroken, and symmetric conical diffraction, it is typically necessary to excite several Dirac cones at once [41]. For the Lieb and kagome lattices, we therefore excited all Dirac points at the corners of the first Brillouin zone, four for the Lieb lattice and six for the kagome lattice [see Figs. 1(d) and 1(f)]; for transition lattices with different θ , we excited the six upper Dirac cones closest to the corners of the first Brillouin zone (see Fig. 6). As an example, the excitation light field for the kagome lattice is shown in Fig. 4 in real and Fourier space.

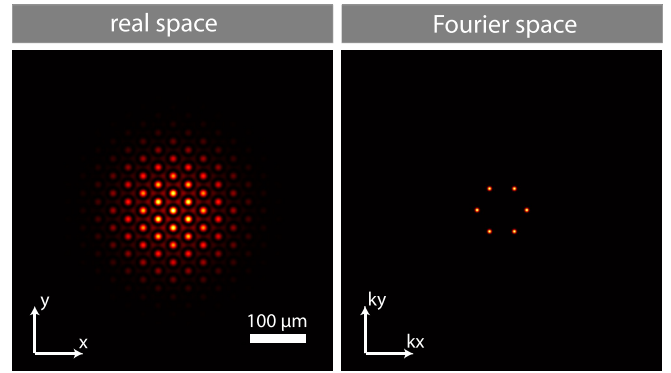


FIG. 4. Excitation light field for the kagome lattice in real and Fourier space, targeting six Dirac cones.

Figure 5 shows the resulting diffraction patterns on the output facets of Lieb-kagome lattices with selected shearing angles θ after a propagation of 60 mm, where the characteristic ring pattern of conical diffraction can be observed for all θ . In the case of the kagome lattice ($\theta = 30^\circ$) and the Lieb lattice ($\theta = 0^\circ$), when the Dirac cones are untilted, the patterns are the most symmetric. In transition states ($30^\circ > \theta > 0^\circ$), the diffraction patterns become elliptic with varying eccentricities. The patterns are twofold mirror symmetric with one symmetry axis in the tilt direction of the upper Dirac

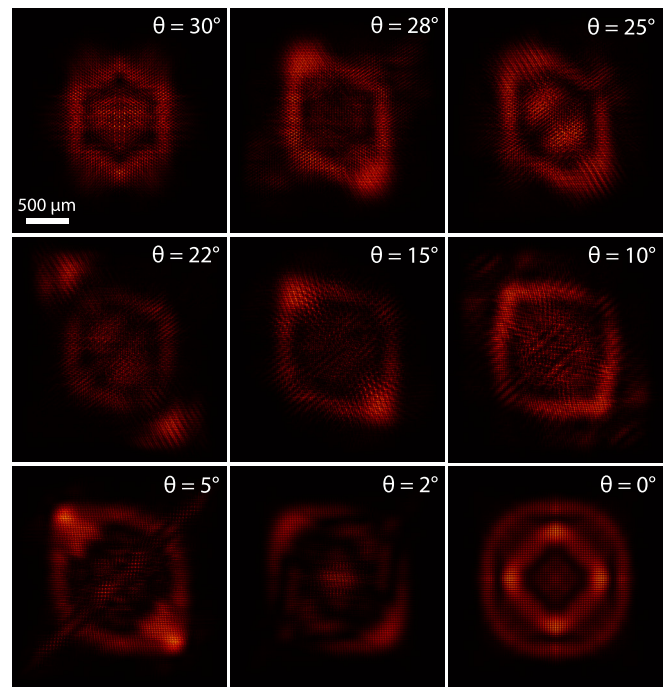


FIG. 5. Diffraction patterns after a propagation of 60 mm through Lieb-kagome lattices with different shearing angles θ , showing asymmetric conical diffraction for $0^\circ < \theta < 30^\circ$. For these patterns, selected Dirac points were excited by a superposition of plane waves. For the cases of regular Dirac cones, the six ($\theta = 30^\circ$), respectively four ($\theta = 0^\circ$), Dirac points at the K/K' points were excited. For all other cases, the six Dirac points closest to the K/K' points were excited.

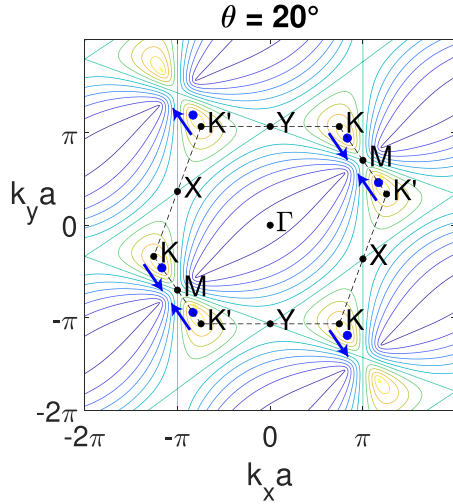


FIG. 6. \mathbf{k} space positions of the upper Dirac points (blue filled circles) of Lieb-kagome lattices in transition states excited to generate conical diffraction. The blue arrows mark the tilt directions of the corresponding Dirac cones.

cones and the other in the tilt direction of the lower Dirac cones, which are perpendicular to each other. In all cases, some light remains in the middle of the ring, which is common with conical diffraction, and is usually attributed to the influence of bands other than those forming the Dirac cones [21]. For very small angles, in Fig. 5 for $\theta = 2^\circ$, the ring pattern is broken: There first appear two separate half-circles moving apart in the tilt direction of the upper Dirac cones, followed by the same in the tilt direction of the lower Dirac cones. We attribute this to the fact that in this case the upper and lower Dirac cones are so close in \mathbf{k} space that our light field excites both at the same time.

When, starting from the Lieb lattice at $\theta = 0^\circ$, θ is increased, each Dirac point of the lattice splits into four, two upper Dirac points and two lower Dirac points, as seen in Figs. 1(d)–1(f). In such a group of four Dirac points, the upper Dirac cones are tilted toward each other, while the lower Dirac cones are tilted away from each other. Of the six Dirac cones excited for the simulations in Fig. 5, three are therefore tilted in one direction and the other three in the opposite direction, as shown in Fig. 6. To show evidence of tilted Dirac cones in the Lieb-kagome lattice, we need to specifically excite only Dirac cones tilted in one direction. The result of this approach is presented in Fig. 7 for lattices with $\theta = 30^\circ$, 25° , and 22° . In the left column, all six Dirac cones shown in Fig. 6 were excited, in the middle column only those tilted diagonally upward, and in the right column only those tilted diagonally downward. The blue (gray) circles in Fig. 7 mark the position and extent of the excitation light fields. When only three Dirac cones are excited, the symmetry of the diffraction patterns is reduced regardless of the shearing angle θ . Nevertheless, in the case of the kagome lattice ($\theta = 30^\circ$), the patterns remain centered on the point where the lattice was excited, as is expected for regular conical diffraction. For $\theta = 25^\circ$ and $\theta = 22^\circ$, in contrast, we observe a clear shift of the diffraction patterns in the tilt direction of the Dirac cones when only

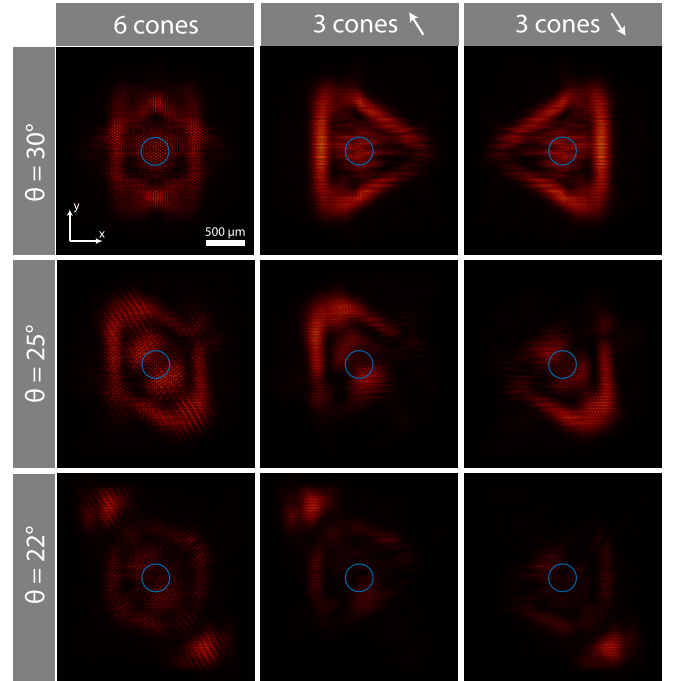


FIG. 7. Diffraction patterns after a propagation of 60 mm through Lieb-kagome lattices with different shearing angles θ , when different selections of Dirac cones are excited. The blue (gray) circles indicate the position and size of the excitation light fields.

cones tilted in one direction are excited. This behavior proves that the Dirac cones in question are indeed tilted [23].

V. EXPERIMENTS IN FUSED SILICA

In order to verify our results experimentally, we fabricated photonic lattices in fused silica (SiO_2) using the direct laser writing technique [26,42]. Table II shows the main differences in parameters compared to the simulations presented so far. Figure 8 shows microscope images of the back facets of two of the lattices we fabricated, one with $\theta = 30^\circ$ (kagome lattice), consisting of 2415 waveguides, and one with $\theta = 25^\circ$, consisting of 1536 waveguides. Our direct laser writing setup uses a pulsed laser with a wavelength of 1030 nm and a pulse length of approximately 250 fs. Waveguides are written by translating the sample in a direction perpendicular to the laser beam (transversally) on a motion-controlled stage. A spatial light modulator (SLM) is used to counteract aberrations and compensate dependencies of the waveguide properties on the depth in the sample. Our setup for probing the resulting photonic lattices uses a continuous wave laser with a central wavelength of 532 nm. An SLM is used to replicate the

TABLE II. Summary of the parameters of experiments and corresponding simulations.

Waveguide dimensions (FWHM)	$3 \mu\text{m} \times 6 \mu\text{m}$
Waveguide distance	$18 \mu\text{m}$
Excitation wavelength	532 nm
Propagation distance	40 mm

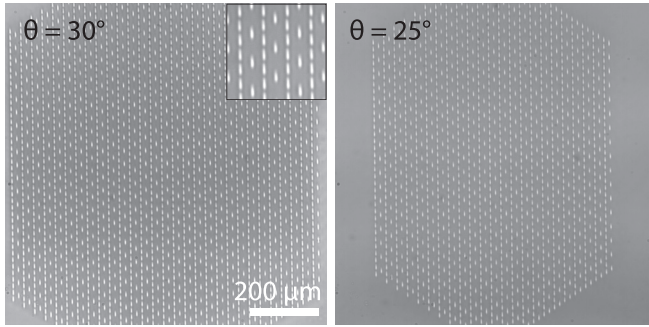


FIG. 8. Back facet of SiO_2 sample with laser-written waveguides, forming two photonic lattices. The inset is a close-up of some waveguides, showing their elliptical cross sections.

light fields used for excitation in the simulations, which were shown in Fig. 4. A more detailed description of both setups, including sketches, can be found in Ref. [42].

A known drawback of using a transversal writing scheme is that the waveguides fabricated this way exhibit elliptical instead of circular cross-sections, which can be seen in the inset of Fig. 8. This effect can currently only be partially compensated for, and known mitigation methods did not prove effective in our case. The elliptical waveguides introduce a small anisotropy in the coupling constants, which slightly deform the band structure of the resulting photonic lattices. Simulations with elliptical waveguides (Fig. 9) show that this causes conical diffraction to degenerate into a line pattern. In order to make patterns comparable for different values of the shearing angle θ , we rotated the lattices by a θ -dependent angle of $\varphi_{\text{rot}} = (90^\circ - \theta)/2 + 90^\circ$, which places the tilt direction of the upper Dirac cones in the y direction and orients the line patterns along the same direction.

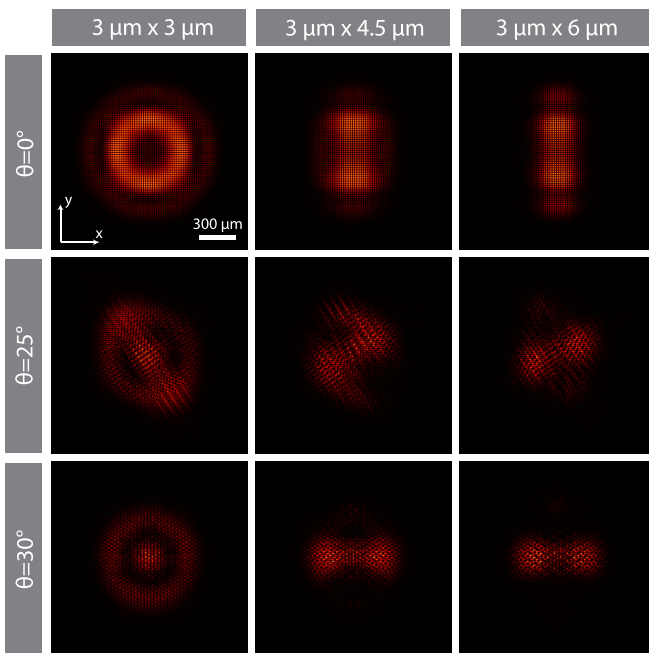


FIG. 9. Simulations demonstrating the deterioration of conical diffraction when the cross section of waveguides changes from circular to elliptical.

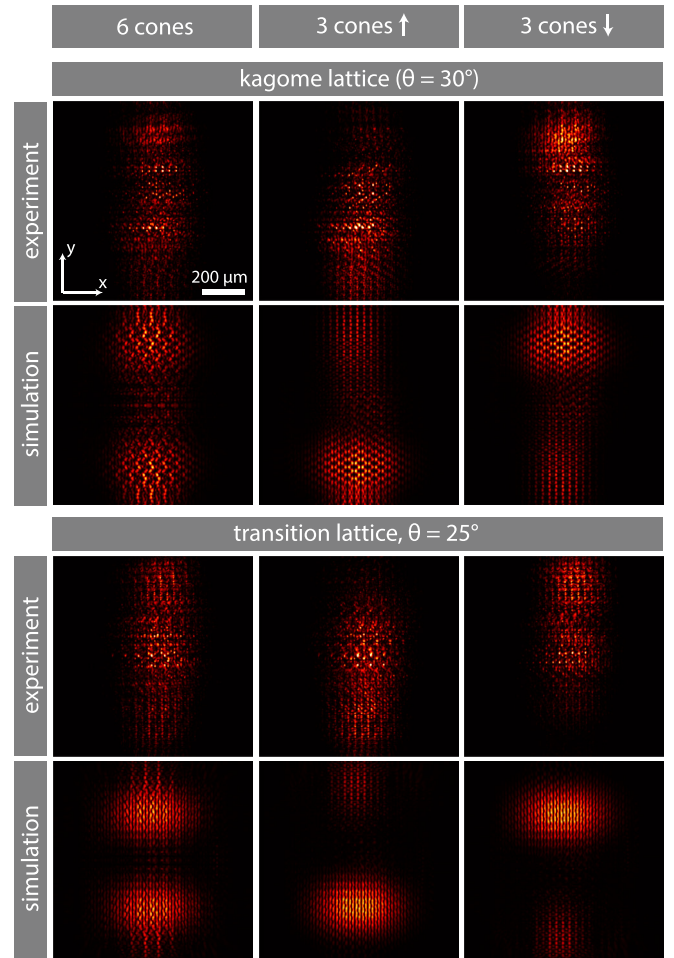


FIG. 10. Diffraction patterns after propagating 40 mm through the lattices shown in Fig. 8, along with simulations for comparison. The same selections of Dirac cones as in Fig. 7 were excited.

Figure 10 shows the diffraction patterns after propagation of 40 mm through the lattices described above, along with simulations using the parameters from Table II for comparison. To show the effect of tilting, the same selections of Dirac cones as in Fig. 7 were excited, which is again shown in the different columns. As discussed above, due to the elliptical cross sections of the waveguides, the patterns are line shaped with one or two bright spots rather than the circular patterns expected for conical diffraction. Nevertheless, in the simulations presented in Fig. 10, the shift of the diffraction patterns' centers in the direction in which the Dirac cones are tilted can still be observed. This is the characteristic for tilted Dirac cones. The images obtained from experiments generally match the simulations, but exhibit more light remaining in the center of the pattern, i.e., not diffracting. We attribute this to distortions of the band structure caused by the waveguides' elliptical cross sections and other experimental inaccuracies.

VI. CONCLUSION

In this work, we have studied the tilted Dirac cones of the Lieb-kagome lattice in depth using the tight-binding method. We have shown how their tilting depends on the shearing

angle θ , which describes the transition between Lieb and kagome lattices and on the relative strength of next-nearest neighbor interaction, and how these parameters can be used to tune the Dirac cones of the lattice to type I, II, or III. This provides future researchers with a way to deliberately engineer these different Dirac cones and use them to study novel phenomena. After that, we studied realizations of Lieb-kagome lattices as photonic lattices using split-step beam propagation simulations. We have shown conical diffraction in transition states between Lieb and kagome lattice, where we found evidence of Dirac cones tilted in different directions.

In a final step, we fabricated on a fused silica chip large-scale photonic lattices consisting of thousands of single-mode waveguides. Although experimental challenges exist in the form of elliptical waveguides instead of circular waveguides, we were able to prove the signature of tilted Dirac cones. We expect that the presented experiments can be further improved by switching to a longitudinal writing scheme or an alternative fabrication technique. Our studies further the understanding of the Lieb-kagome lattice and tilted Dirac cones in general and provide a basis for further research into these subjects.

-
- [1] K. S. Novoselov, A. K. Geim, S. V. Morozov, D. Jiang, Y. Zhang, S. V. Dubonos, I. V. Grigorieva, and A. A. Firsov, Electric field effect in atomically thin carbon films, *Science* **306**, 666 (2004).
- [2] A. H. Castro Neto, F. Guinea, N. M. R. Peres, K. S. Novoselov, and A. K. Geim, The electronic properties of graphene, *Rev. Mod. Phys.* **81**, 109 (2009).
- [3] T. O. Wehling, A. M. Black-Schaffer, and A. V. Balatsky, Dirac materials, *Adv. Phys.* **63**, 1 (2014).
- [4] S. A. Yang, Dirac and Weyl materials: Fundamental aspects and some spintronics applications, *SPIN* **06**, 1640003 (2016).
- [5] J. Wang, S. Deng, Z. Liu, and Z. Liu, The rare two-dimensional materials with Dirac cones, *Natl. Sci. Rev.* **2**, 22 (2015).
- [6] D. Leykam and A. S. Desyatnikov, Conical intersections for light and matter waves, *Adv. Phys. X* **1**, 101 (2016).
- [7] P. Menz, H. Hanafi, J. Imbrock, and C. Denz, Noncontractible loop states from a partially flat band in a photonic borophene lattice, [arXiv:2211.10255](https://arxiv.org/abs/2211.10255)
- [8] P. Menz, H. Hanafi, D. Leykam, J. Imbrock, and C. Denz, Pseudospin-2 in photonic chiral borophene, [arXiv:2212.00204](https://arxiv.org/abs/2212.00204).
- [9] M. Milićević, G. Montambaux, T. Ozawa, O. Jamadi, B. Real, I. Sagnes, A. Lemaître, L. Le Gratiet, A. Harouri, J. Bloch, and A. Amo, Type-III and Tilted Dirac Cones Emerging from Flat Bands in Photonic Orbital Graphene, *Phys. Rev. X* **9**, 031010 (2019).
- [10] T. Kawarabayashi, Y. Hatsugai, T. Morimoto, and H. Aoki, Generalized chiral symmetry and stability of zero modes for tilted Dirac cones, *Phys. Rev. B* **83**, 153414 (2011).
- [11] T. Cheng, H. Lang, Z. Li, Z. Liu, and Z. Liu, Anisotropic carrier mobility in two-dimensional materials with tilted Dirac cones: Theory and application, *Phys. Chem. Chem. Phys.* **19**, 23942 (2017).
- [12] H. Huang, K.-H. Jin, and F. Liu, Black-hole horizon in the Dirac semimetal $\text{Zn}_2\text{In}_2\text{S}_5$, *Phys. Rev. B* **98**, 121110(R) (2018).
- [13] C. Sims, Topologically protected wormholes in type-III Weyl semimetal $\text{Co}_3\text{In}_2\text{X}_2$ ($X = \text{S}, \text{Se}$), *Condens. Matter* **6**, 18 (2021).
- [14] A. Szameit and S. Nolte, Discrete optics in femtosecond-laser-written photonic structures, *J. Phys. B: At. Mol. Opt. Phys.* **43**, 163001 (2010).
- [15] J. Imbrock, H. Hanafi, M. Ayoub, and C. Denz, Local domain inversion in MgO-doped lithium niobate by pyroelectric field-assisted femtosecond laser lithography, *Appl. Phys. Lett.* **113**, 252901 (2018).
- [16] H. Hanafi, S. Kroesen, G. Lewes-Malandrakis, C. Nebel, W. H. Pernice, and C. Denz, Polycrystalline diamond photonic waveguides realized by femtosecond laser lithography, *Opt. Mater. Express* **9**, 3109 (2019).
- [17] J. Imbrock, D. Szalek, S. Laubrock, H. Hanafi, and C. Denz, Thermally assisted fabrication of nonlinear photonic structures in lithium niobate with femtosecond laser pulses, *Opt. Express* **30**, 39340 (2022).
- [18] M. C. Rechtsman, J. M. Zeuner, Y. Plotnik, Y. Lumer, D. Podolsky, F. Dreisow, S. Nolte, M. Segev, and A. Szameit, Photonic Floquet topological insulators, *Nature (London)* **496**, 196 (2013).
- [19] F. Dreisow, A. Szameit, M. Heinrich, T. Pertsch, S. Nolte, A. Tünnermann, and S. Longhi, Bloch-Zener Oscillations in Binary Superlattices, *Phys. Rev. Lett.* **102**, 076802 (2009).
- [20] S. Longhi, M. Marangoni, M. Lobino, R. Ramponi, P. Laporta, E. Cianci, and V. Foglietti, Observation of Dynamic Localization in Periodically Curved Waveguide Arrays, *Phys. Rev. Lett.* **96**, 243901 (2006).
- [21] O. Peleg, G. Bartal, B. Freedman, O. Manela, M. Segev, and D. N. Christodoulides, Conical Diffraction and Gap Solitons in Honeycomb Photonic Lattices, *Phys. Rev. Lett.* **98**, 103901 (2007).
- [22] F. Diebel, D. Leykam, S. Kroesen, C. Denz, and A. S. Desyatnikov, Conical Diffraction and Composite Lieb Bosons in Photonic Lattices, *Phys. Rev. Lett.* **116**, 183902 (2016).
- [23] H. Zhong, R. Wang, M. R. Belić, Y. Zhang, and Y. Zhang, Asymmetric conical diffraction in dislocated edge-centered square lattices, *Opt. Express* **27**, 6300 (2019).
- [24] R. A. Vicencio, C. Cantillano, L. Morales-Inostroza, B. Real, C. Mejía-Cortés, S. Weimann, A. Szameit, and M. I. Molina, Observation of Localized States in Lieb Photonic Lattices, *Phys. Rev. Lett.* **114**, 245503 (2015).
- [25] Y. Zong, S. Xia, L. Tang, D. Song, Y. Hu, Y. Pei, J. Su, Y. Li, and Z. Chen, Observation of localized flat-band states in kagome photonic lattices, *Opt. Express* **24**, 8877 (2016).
- [26] H. Hanafi, P. Menz, A. McWilliam, J. Imbrock, and C. Denz, Localized dynamics arising from multiple flat bands in a decorated photonic Lieb lattice, *APL Photon.* **7**, 111301 (2022).
- [27] D. Leykam, O. Bahat-Treidel, and A. S. Desyatnikov, Pseudospin and nonlinear conical diffraction in Lieb lattices, *Phys. Rev. A* **86**, 031805(R) (2012).
- [28] X. Liu, J. Yang, X. Guo, J. Zhang, P. Li, and Y. Liu, Conical diffractions in kagome lattice, *Results Phys.* **23**, 104007 (2021).
- [29] H. Zhong, R. Wang, F. Ye, J. Zhang, L. Zhang, Y. Zhang, M. R. Belić, and Y. Zhang, Topological insulator properties of

- photonic kagome helical waveguide arrays, *Results Phys.* **12**, 996 (2019).
- [30] K. Asano and C. Hotta, Designing Dirac points in two-dimensional lattices, *Phys. Rev. B* **83**, 245125 (2011).
- [31] W. Jiang, M. Kang, H. Huang, H. Xu, T. Low, and F. Liu, Topological band evolution between Lieb and kagome lattices, *Phys. Rev. B* **99**, 125131 (2019).
- [32] L.-K. Lim, J.-N. Fuchs, F. Piéchon, and G. Montambaux, Dirac points emerging from flat bands in Lieb-kagome lattices, *Phys. Rev. B* **101**, 045131 (2020).
- [33] K. Jin, H. Zhong, Y. Li, F. Ye, Y. Zhang, F. Li, C. Liu, and Y. Zhang, Parametric type-II Dirac photonic lattices, *Adv. Quantum Technol.* **3**, 2000015 (2020).
- [34] H. Zhong, S. Xia, Y. Zhang, Y. Li, D. Song, C. Liu, and Z. Chen, Nonlinear topological valley Hall edge states arising from type-II Dirac cones, *Adv. Photon.* **3**, 056001 (2021).
- [35] Y.-G. Chen, X. Luo, F.-Y. Li, B. Chen, and Y. Yu, Quantum chaos associated with an emergent ergosurface in the transition layer between type-I and type-II Weyl semimetals, *Phys. Rev. B* **101**, 035130 (2020).
- [36] A. Sharma and A. Agrawal, New method for nonparaxial beam propagation, *J. Opt. Soc. Am. A* **21**, 1082 (2004).
- [37] M. O. Goerbig, J.-N. Fuchs, G. Montambaux, and F. Piéchon, Tilted anisotropic Dirac cones in quinoïd-type graphene and α -(BEDT-TTF)₂I₃, *Phys. Rev. B* **78**, 045415 (2008).
- [38] A. El Hassan, F. K. Kunst, A. Moritz, G. Andler, E. J. Bergholtz, and M. Bourennane, Corner states of light in photonic waveguides, *Nat. Photon.* **13**, 697 (2019).
- [39] M. R. Slot, T. S. Gardenier, P. H. Jacobse, G. C. Van Miert, S. N. Kempkes, S. J. Zevenhuizen, C. M. Smith, D. Vanmaekelbergh, and I. Swart, Experimental realization and characterization of an electronic Lieb lattice, *Nat. Phys.* **13**, 672 (2017).
- [40] Z. Li, J. Zhuang, L. Wang, H. Feng, Q. Gao, X. Xu, W. Hao, X. Wang, C. Zhang, K. Wu *et al.*, Realization of flat band with possible nontrivial topology in electronic kagome lattice, *Sci. Adv.* **4**, eaau4511 (2018).
- [41] M. J. Ablowitz, S. D. Nixon, and Y. Zhu, Conical diffraction in honeycomb lattices, *Phys. Rev. A* **79**, 053830 (2009).
- [42] H. Hanafi, P. Menz, and C. Denz, Localized states emerging from singular and nonsingular flat bands in a frustrated fractal-like photonic lattice, *Adv. Opt. Mater.* **10**, 2102523 (2022).

Correction: A production coding error in the notation (SiO₂) in the penultimate sentence of the abstract in the HTML version of the article resulted in the omission of the subscript 2. It has now been fixed.